Efficient Access to Functionalized Mesoporous Materials with Bicontinuous Morphologies via Kinetic Approach

Jun Yuan[a,b,c], Xiang Liu[b,c], Yingying Wang[b,c], Tao Wen[b,c*]

[a] Center for Electron Microscopy, South China University of Technology, Guangzhou 510640, China

[b] School of Emergent Soft Matter, South China University of Technology, Guangzhou 510640, China

[c] Guangdong Provincial Key Laboratory of Functional and Intelligent Hybrid Materials and Devices, South China University of Technology, Guangzhou 510640, China

*To whom correspondence should be addressed. E-mail: twen@scut.edu.cn (T.W.)

Abstract

In this work, we developed an approach that can simultaneously control the morphology and pore-surface chemistry of mesoporous materials. By introducing diols as 'non-covalent cross-linking agents', microphase separation of polystyrene-*b*-poly(4-vinylpyridine)-*b*-polylactide triblock terpolymers can be tuned, leading to the formation of long-lived metastable phase with disordered bicontinuous morphology. After removing polylactide end-block by selectively etching, mesoporous structures can be achieved, but poly(4-vinylpyridine) mid-blocks will be preserved on the inner wall of pores. We demonstrate that the prepared mesoporous materials can be applied as adsorbents for organic dyes and metal ions. This work provides new insight into the development of functionalized mesoporous materials.

For Table of Contents Only

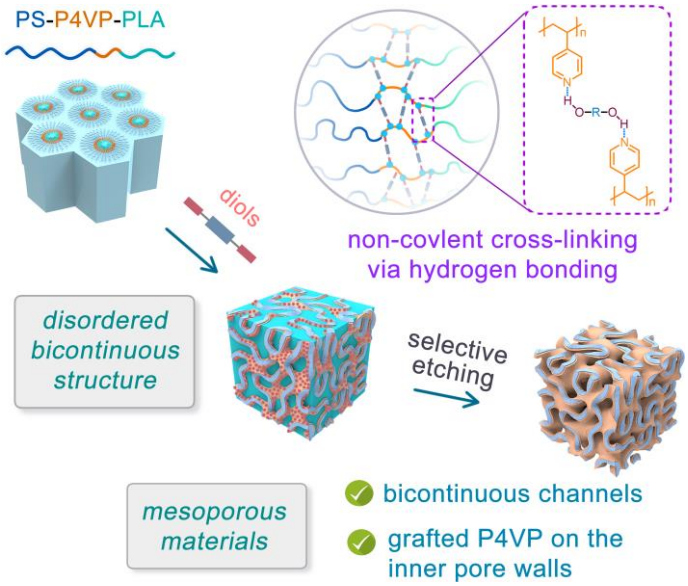

Introduction

Over the past few decades, mesoporous materials with pore sizes in the range of 2 to 50 nm have garnered widespread attention due to their high surface area and efficient transport capabilities.[1-3] So far, the preparation of mesoporous materials has evolved through numerous methods.[4-7] In these methods, the phase structure of block copolymers is often employed to construct mesoporous materials.[8-10] Block copolymers can form mesopores morphology after undergoing appropriate etching processes, and they can also be used in combination with other functional components as templates or directing agents.[11, 12]

The chemical properties of the pore walls, i.e., inner surface, play a crucial role in determining the final performance and functionality of mesoporous materials.[13, 14] Currently, there are two commonly used methods to modify or functionalize pore-wall surface. For one thing, post-modification is a straight forward approach to functionalize pore walls. In this case, functional groups will be introduced onto the pre-designed framework after the preparation of porous materials.[15-17] For another thing, inherent functional groups on the pore walls can be introduced during the pore formation process. In particular, by rational designing topological structure of block copolymers, mesoporous materials with grafted polymers on the pore walls can be prepared.[18] For instance, for ABC triblock terpolymer with a degradable end-block, mid-block-grafted mesopores is able to be prepared by removing end-block after selectively etching. For example, Hillmyer and co-workers reported the preparation of hydrophilic mesoporous materials using polylactide-*b*-poly(*N,N*-dimethylacrylamide)-*b*-polystyrene (PLA-

PDMA-PS).[19, 20] Also, Ndoni and co-workers reported nanoporous materials with hydrophilic pore walls from polydimethylsiloxane-*b*-poly(*tert*-butyl acrylate)-*b*-polystyrene (PDMS-PtBA-PS).[21]

In addition to the chemical properties of the pore walls, the tortuosity and continuity of the pores in mesoporous materials also play a crucial role in their performance. Self-assembly of block copolymers can lead to various morphologies, including alternating lamellar (L), hexagonally packed cylindrical (HC), and spherical (S) structures.[22] Furthermore, self-assembly of block copolymers can also lead to three distinct structurally continuous cubic geometries: double gyroid (G), double diamond (D), and plumber's nightmare (P).[23-26] The transport efficiency of mesoporous materials prepared from block copolymers can be quantified using the morphology factor (f). The f values for S, C, G/D/P, and L structures are 0, 1/3, 1, and 2/3, respectively.[27-29] This implies that G/D/P phase structures possess higher interparticle transport efficiency, due to their three-dimensional uninterrupted pathways. Furthermore, the tortuosity factor (τ) of the G/D/P phases is also higher than that of other ones, giving a larger specific surface area.[28, 30-32] However, it is challenging to prepare bicontinuous nanostructures by self-assembly of block copolymers, since thermodynamically stable phases of block copolymers (G/D/P) only exist in very narrow regions.[33-36] Recently, we developed a strategy for the preparation of bicontinuous structures by controlling the kinetics of microphase separation.[37]

In this study, we reported the preparation of bicontinuous mesopores with functionalized pore walls. We designed and synthesized a triblock terpolymer,

polystyrene-*b*-poly(4-vinylpyridine)-*b*-polylactide (PS-P4VP-PLA). By introducing diol molecules as 'non-covalent cross-linkers', bicontinuous nanostructures can be induced via self-assembly of SVA. After selectively removing PLA end-block, bicontinuous mesopores can be obtained. Moreover, due to the presence of surface-grafted P4VP on the pore walls, the prepared porous materials exhibited adsorption capacities for organic dyes and metallic ions.

Results and discussion

PS-P4VP-PLA triblock copolymer, named as SVA, was synthesized by using the reversible addition-fragmentation chain transfer (RAFT) and ring-opening polymerization (ROP). The detailed procedures were described in the Supporting Information (SI). The synthesized triblock copolymer was characterized using gel permeation chromatography (GPC) and proton nuclear magnetic resonance (^{1}H NMR) (Figures S2 and S3). The molecular weights (M_n) of P4VP, PS-P4VP-OH, and SVA are 5800 g/mol, 33300 g/mol, and 53100 g/mol, respectively. The volume fractions of PS, P4VP, and PLA in SVA are 64%, 8%, and 28%, respectively (Table S1). Note that the accurate M_n value of P4VP is calculated based on ^{1}H NMR result (Figure S1).

Self-assembly of block copolymers is driven by the immiscibility of different blocks, which can be defined by the product of the Flory-Huggins interaction parameter (χ) and the degree of polymerization (N).[38-40] The χ value between PS and P4VP at 25 °C is reported to be 0.56.[41] Also, the microphase separation between P4VP and PLA has been reported previously.[42] Figure 1a shows the SAXS curves of synthesized SVA

before and after selective etching with 2M NaOH solution (MeOH/water = 50:50 *v*/*v*). It is found that the reflection peaks can be observed at a relative *q* value of 1 : √7 in the pristine SVA. After removing PLA microdomains, more reflection peaks can be observed at relative *q* values of 1 : √3 : √4 : √7 : √9, due to the enhanced electron contrast. Also, the SAXS results indicate the formation of hexagonally packed cylinders by the self-assembly of SVA. Figure 1b shows the corresponding transmission electron microscopy (TEM) micrograph of SVA stained by I_2, in which spot-like patterns with hexagonal symmetry can be observed. By taking a closer look on the TEM micrograph, ring-like morphology can be recognized, resulting from the strained P4VP mid-block (the arrows in Figure 1b). It indicates that core-shell cylinder structures were formed by pure SVA. Moreover, the corresponding SEM micrograph exhibits typical cylinder structures in the etched SVA (Figure 1c), which is consistent with the above results.

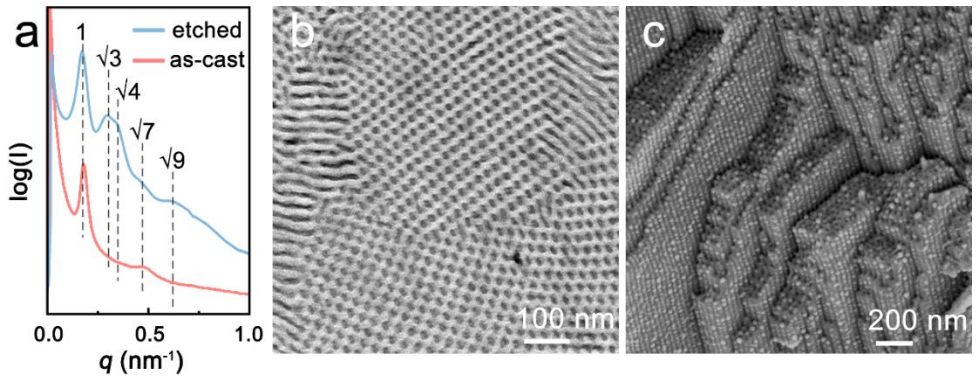

Figure 1. (a) SAXS profiles of as-cast and etched SVA. (b) TEM micrograph of as-cast SVA stained by I_2. (c) SEM micrograph of etched SVA.

As shown above, after selective etching, porous structure can be achieved. To clarify whether P4VP mid-block was removed during etching, SVA etched for different times were measured by ^{1}H NMR. As shown in Figure 2, the peak at around 5.2 ppm is

attributed to the methine protons (-CH) of the PLA, while the peak around 8.3 ppm is associated with the protons on the pyridine rings of P4VP. It is found that PLA can be completely removed after etching for 3 hours (Figure 2). Yet, the molar fraction of P4VP in the etched SVA is almost independent with the etching time, indicating that P4VP mid-blocks were not cut off from PS matrix during etching. Also, these results confirm the presence of grafted P4VP on the inner surface of mesopores in the etched SVA.

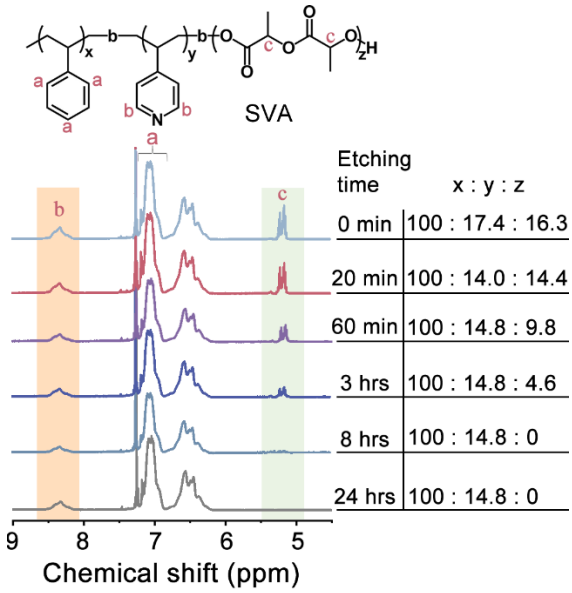

Figure 2. ^{1}H NMR spectra of SVA etched with 2M NaOH (MeOH/water = 50:50 *v*/*v*) for different times, and the corresponding monomer ratios of PS, P4VP, and PLA blocks.

Next, we intend to control the self-assembled morphologies of SVA. To this end, three diol molecules, *i.e.*, ethylene glycol (EG), neopentyl glycol (NPG), and bis(4-hydroxyphenyl) sulfone (BPS), were doped into SVA by solution mixing. In the following study, the composites of SVA doped with NPG/EG/BPS are termed as SVA/N*x*, SVA/E*x*, and SVA/B*x*, respectively, where *x* represents the doping

concentration of diols (w_{diol}/w_{SVA}). After etching, the corresponding porous materials are denoted as 'eSVA/N*x*', 'eSVA/E*x*', and 'eSVA/B*x*', respectively. For example, 'eSVA/N0' refers to pure SVA after etching, and 'eSVA/N5' refers to NPG-doped SVA with doping concentration of 5% after etching.

Firstly, the self-assembled morphologies of SVAs in the presence of NPG were investigated. Figures 3a-3d show the TEM micrographs of self-assembled SVAs doped with NPG, in which the dark regions represent the P4VP domains. It is found that the introducing of NPG can effectively regulate the intrinsic morphology of SVA. With the increasing of doping concentration, the self-assembled structures of SVA gradually transfer from cylinder to lamellar. Interestingly, as the doping concentration of NPG is below 10%, self-assembled nanostructures with isotropic morphology can be observed, e.g., SVA/N5 (Figure 3a). To achieve a statistical description on the TEM microscope, their fast Fourier transform (FFT) patterns were analyzed. For SVA/N5 and SVA/N10, ring-like FFT patterns can be observed. In contrast, the FFT pattern of SVA/N20 shows hexagonally arranged spots, and highly aligned spots can be obtained from the TEM microscope of SVA/N40, due to the oriented textures on TEM micrographs (see more details in SI, Figure S4). These results are consistent with the TEM real-space observation. Again, it suggests that continuous but disordered nanostructures can be self-assembled by SVA in the presence of NPG at certain concentration. According to TEM and SEM observation, the phase diagram of SVA/NPG can be determined as shown in Figure 4.

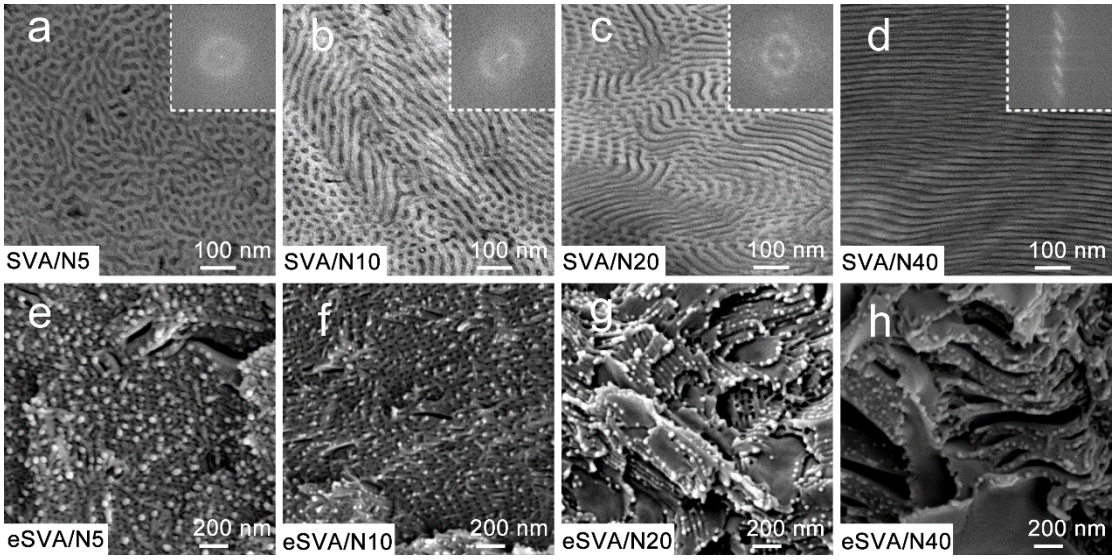

Figure 3. TEM micrographs of SVAs doped with NPG (a-d), and the corresponding SEM micrographs of NPG-doped SVAs after etching (e-h).

To further investigate the morphological evolution of SVA with NPG dopant, SEM observations on the etched SVAs were performed. Figures 3e-3h show the SEM micrographs of SVA doped with NPG after removing PLA domains. In eSVA/N5, disordered pores can be observed (Figure 3e), rather than cylinder phase observed in eSVA/N0 (see Figure 1c). Also, as the doping concentration exceeds 30%, a lamellar morphology can be observed due to the collapse and compression of the phase structure after removing the PLA domains (Figure 3h). Moreover, when the concentration of NPG is higher than 70%, inversed cylinder structures can be observed (Figure S5). To confirm whether the NPG dopant additive was completely removed during etching, etched SVA/NPG composites were examined by ^{1}H NMR. It is confirmed that most of NPG can be removed within 1 hour (Figure S6). In addition, the morphologies of self-assembled SVA/NPG composites before and after etching were examined by SAXS. It

is observed that the intensity of SAXS peaks is enhanced after etching (Figure S7). In particular, the etched SVA/NPG composites exhibited broad scattering peaks, which is consistent with the disordered morphologies observed in TEM and SEM. However, it is challenging to determine the structures according to the SAXS results, due to the broad scattering peaks.

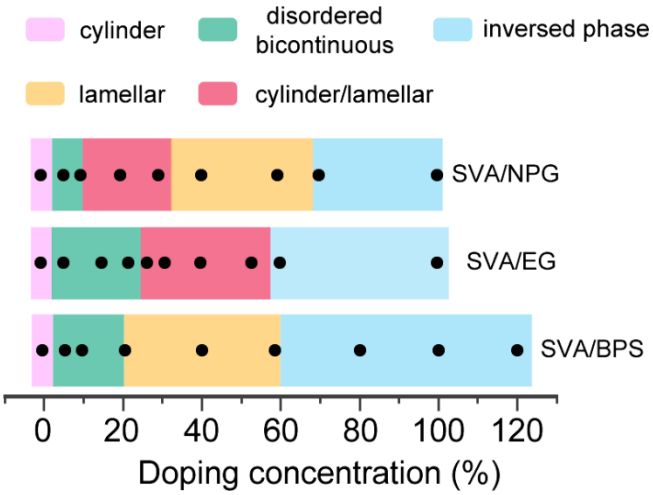

Figure 4. Phase diagrams of SVA/NPG, SVA/EG, and SVA/BPS.

To gain a deeper insight into the mechanism on the controlled self-assemblies of SVA, FTIR spectroscopy is used to determine the inter-molecular interactions between SVA and NPG. Figure S8 shows the FTIR curves of SVA, NPG, and SVA/N10 before and after etching. In the FTIR spectrum of SVA, the peak at round 993 cm^{-1} is associated with the stretching mode of the pyridine rings.[43, 44] However, this peak is significantly weakened in the presence of NPG. Also, the stretching band of pyridine rings shifts to the higher wavenumber[44], due to the coordination of NPG with pyridine rings. For the same reason, the characteristic peaks of NPG at 2971, 2928, and 2882 cm^{-1} are not visible in SVA/N10.[45] The above results indicate that, in the SVA/NPG

composites, the diol molecules interact with the pyridine rings of P4VP mid-segments through hydrogen bonding (Scheme 1). Consequently, the block copolymers were 'non-covalently' crosslinked by the diols, resulting in the reduced chain mobility and reduced kinetics of microphase separation.[46] It leads to the generation of long-lived metastable phase with network morphologies during solution casting. After selective etching, mesoporous bulks with bicontinuous channels and grafted P4VP segments on the inner pore walls can be achieved.

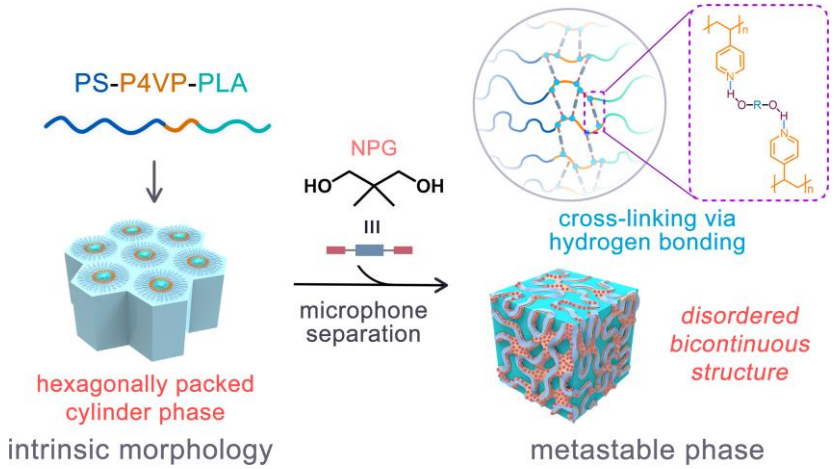

Scheme 1. Mesoporous materials with disordered bicontinuous channels from controlled self-assembly of PS-P4VP-PLA triblock copolymer.

Next, to investigate the structural feature of mesopores, the surface area and pore size distribution of eSVA/N5 are determined by using N_2 sorption technique.[47, 48] The surface areas of mesopores can be calculated using the Brunauer-Emmett-Teller (BET) theory. The BET surface area of eSVA/N5 is measured as 52.2 m^2/g, that is higher than that of eSVA/N0 (46.6%) and eSV/N40 (7.7 m^2/g) (Figure 5). The results indicate that mesopores with a disorder bicontinuous morphology have a larger surface area

compared to cylinder mesopores in eSVA/N0. The relatively lower surface area of eSV/N40 is attributed to the collapse of the lamellar structure after etching. Also, the N_2 sorption isotherm of eSVA/N5 exhibits a type IV isotherm characteristic, indicating the formation of a mesoporous structure (Figure 5b).[49] Furthermore, the abrupt increase in nitrogen adsorption at P/P^0 = 0.88 indicates the presence of a significant outer surface.[50] While the adsorption isotherm exhibits an H1-type hysteresis loop, indicating a relatively narrow pore size distribution. The average pore diameter of eSVA/N5 was calculated using the Barrett-Joyner-Halenda (BJH) method and found to be around 20 nm (inset in Figure 5b).

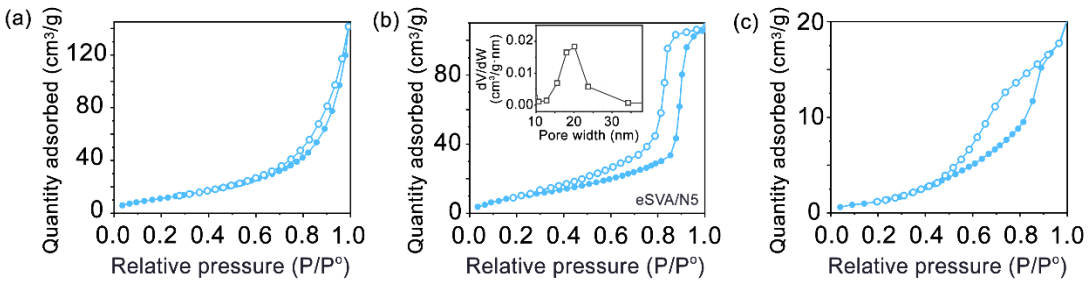

Figure 5. Nitrogen adsorption/desorption isotherms of eSVA/N0 (a), eSVA/N5 (b), and eSVA/N40 (c) (filled circle: adsorption branch; unfilled circle: desorption branch). Insert: pore size distribution.

The above results indicate that bicontinuous morphologies of SVA can be prepared by introducing diol molecules. Besides NPG, it is expected that the other diols can also be applied to control the self-assemblies of SVA. To this end, the self-assemblies of SVA in the presence of EG and BPS were investigated. Figure S9 shows the TEM micrographs of SVA/EG and SVA/BPS composites, and the corresponding SEM micrographs of etched SVA/EG and SVA/BPS were shown in Figure S10 (see also

Figures S11-S12). The SAXS profiles of SVA/EG and SVA/BPS before and after are shown in Figures S13 and S14. It is found that disordered bicontinuous structures can be prepared in both of SVA/EG and SVA/BPS at certain doping concentration, and the corresponding phase diagrams were shown in Figure 4. These results confirm that various diols can reduce the kinetics of microphase separation of SVA, leading to the formation of bicontinuous structures.

We have already demonstrated that mesoporous structures with bicontinuous morphology can be prepared by self-assembly of SVA triblock copolymer under kinetic controlling. More importantly, the preserved P4VP segments grafting on the pore-wall make the porous materials able to adsorb organic dyes and metallic ions.[51, 52] To this end, Orange G (OG) and Cu^{2+} were used to verify the adsorption properties of the porous materials. We also prepared mesoporous PS bulk without P4VP decoration as a control, termed as eSA (Figure S15). To measure the adsorption properties, eSVA/N5 and eSA were immersed in aqueous solutions of OG and Cu^{2+} for varying time intervals, and UV-vis spectroscopy tests were conducted (Figures S16 and S17). Figure 6 shows adsorption capacities of OG and Cu^{2+} ion by eSVA/N5 and eSA. It is found that the adsorption capacities increase and gradually reach saturation, due to the diffusion of dye molecules and ions in the grafted layer of P4VP. This is consistent with the previous report.[53] The equilibrium adsorption capacity (q_e) of mesoporous materials for OG and Cu^{2+} ion at different time intervals can be calculated based on the standard curves (Figures S18 and S19). The equilibrium adsorption capacities of OG and Cu^{2+} by eSV/N5 are 7.5 mg/g and 13.2 mg/g, respectively. In contrast, no adsorption on OG and

Cu^{2+} ion can be detected in eSA, confirming that the adsorption capacity of eSVA/N5 is attributed to the presence of P4VP segments grafting on the pore walls.

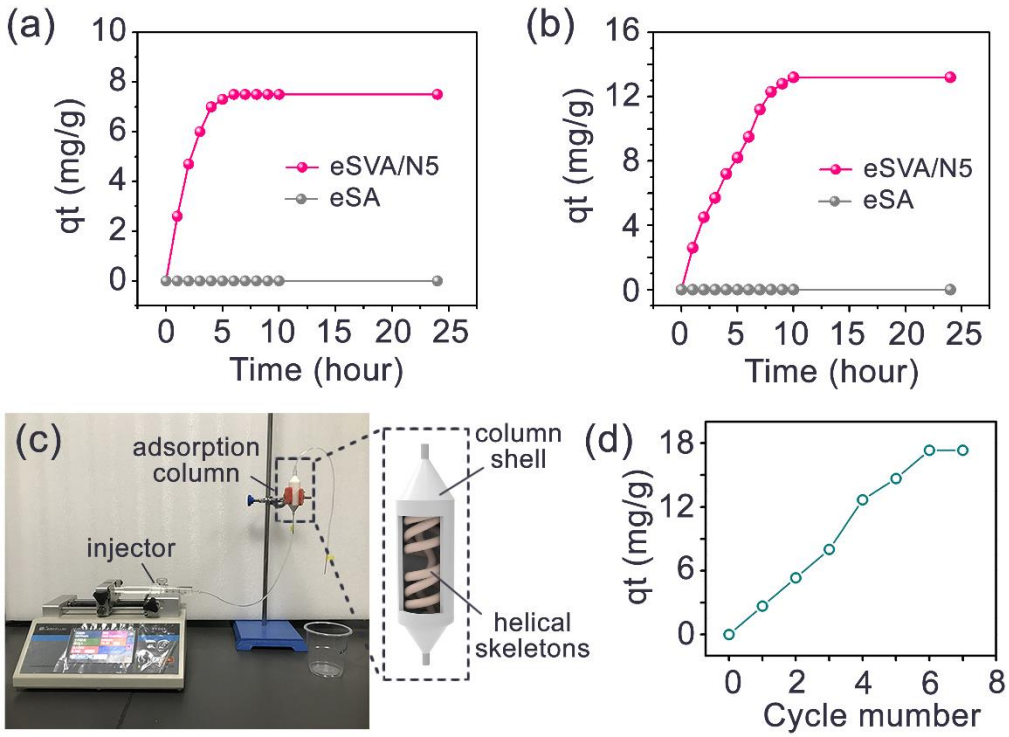

Figure 6. Adsorption capacity curves eSVA/N5 and eSA for OG (a) and Cu^{2+} (b). The photograph and schematic diagram of the home-made adsorption setup (c), and the total adsorption capacity after multiple elution (d).

Moreover, taking advantage of solution processing, mesoporous PS bulk with P4VP decoration can be prepared onto solid substrates as coating layer. To this end, an adsorption column containing several inner helical skeletons was prepared by 3D printing (Figure 6c). By injecting SVA/N5 solution into the column, the composite can be coated onto the surface of the helical skeletons. After etching, porous coating layers can be obtained (Figure S20). Then, the solution of OG was slowly passed through the column by using a syringe pump, and the filtrate was repeatedly passed through the

column for seven times. As shown in Figure 6d, the adsorption reaches equilibrium after passing the column for 6 times, and the equilibrium adsorption capacity is 17.3 mg/g. It is noteworthy that, as it is challenging to control the evaporation rate of SVA/NPG solution in the column, more work is need to further optimize the morphology of coated SVA layer. The follow-up research is ongoing in our laboratory.

Conclusions

In this study, we have reported an approach for the fabrication of morphology-controlled mesoporous materials with P4VP-functionalized pore walls. In the presence of diols as 'non-covalent cross-linking agents', e.g., NPG, EG, and BPS, the self-assemblies of PS-P4VP-PLA triblock terpolymer (SVA) can be effectively retarded, due to the coordination of OH groups of diols and pyridine rings of mid-block. Consequently, the morphologies of self-assembled SVA can be regulated. In particular, under certain doping concentration, disordered bicontinuous morphologies can be achieved. After selective etching, mesoporous bulks with network channels and P4VP-grafted inner surfaces can be obtained. The mesoporous materials exhibit adsorption capabilities for organic dyes and metal ions. This work provides new insight into the development of functional mesoporous materials.

Supporting Information

Experimental methods, additional SEM micrographs, SAXS profiles, NMR spectra, and FT-IR spectra.

Notes

The authors declare no competing financial interest.

Acknowledgements

We acknowledge the support from the Fundamental Research Funds for the Central Universities (2023ZYGXZR107), and the TCL science and technology innovation fund.

Reference

1. Scott, B. J.; Wirnsberger, G.;Stucky, G. D. *Chemistry of materials* **2001,** *13*, 3140.
2. Wu, D.; Xu, F.; Sun, B.; Fu, R.; He, H.;Matyjaszewski, K. *Chemical reviews* **2012,** *112*, 3959.
3. Liang, C.; Li, Z.;Dai, S. *Angewandte Chemie International Edition* **2008,** *47*, 3696.
4. Wan, Y.;Zhao *Chemical reviews* **2007,** *107*, 2821.
5. Wang, S. *Microporous and mesoporous materials* **2009,** *117*, 1.
6. Ma, T.-Y.; Liu, L.;Yuan, Z.-Y. *Chemical Society Reviews* **2013,** *42*, 3977.
7. Wu, S.-H.; Mou, C.-Y.;Lin, H.-P. *Chemical Society Reviews* **2013,** *42*, 3862.
8. Hillmyer, M. A. *Block copolymers II* **2005**, 137.
9. Li, C.; Li, Q.; Kaneti, Y. V.; Hou, D.; Yamauchi, Y.;Mai, Y. *Chemical Society Reviews* **2020,** *49*, 4681.
10. de AA Soler-Illia, G. J.; Crepaldi, E. L.; Grosso, D.;Sanchez, C. *Current Opinion in Colloid & Interface Science* **2003,** *8*, 109.
11. Petkovich, N. D.;Stein, A. *Chemical Society Reviews* **2013,** *42*, 3721.
12. Thomas, A.; Goettmann, F.;Antonietti, M. *Chemistry of Materials* **2008,** *20*, 738.
13. Gamys, C. G.; Schumers, J. M.; Mugemana, C.; Fustin, C. A.;Gohy, J. F. *Macromolecular rapid communications* **2013,** *34*, 962.
14. Salonen, J.;Lehto, V.-P. *Chemical engineering journal* **2008,** *137*, 162.
15. Vilela, F.; Zhang, K.;Antonietti, M. *Energy & Environmental Science* **2012,** *5*, 7819.
16. Sun, Q.; Dai, Z.; Meng, X.;Xiao, F.-S. *Chemical Society Reviews* **2015,** *44*, 6018.
17. Sagitha, P.; Reshmi, C.; Sundaran, S. P.;Sujith, A. *European Polymer Journal* **2018,** *105*, 227.
18. Mao, H.; Arrechea, P. L.; Bailey, T. S.; Johnson, B. J.;Hillmyer, M. A. *Faraday discussions* **2005,** *128*, 149.
19. Rzayev, J.;Hillmyer, M. A. *Journal of the American chemical society* **2005,** *127*, 13373.
20. Rzayev, J.;Hillmyer, M. A. *Macromolecules* **2005,** *38*, 3.
21. Guo, F.; Jankova, K.; Schulte, L.; Vigild, M. E.;Ndoni, S. *Macromolecules* **2008,** *41*, 1486.
22. Bates, F. S.;Fredrickson, G. H. *Annual review of physical chemistry* **1990,** *41*, 525.
23. Lin, Z.; Liu, S.; Mao, W.; Tian, H.; Wang, N.; Zhang, N.; Tian, F.; Han, L.; Feng, X.;Mai, Y. *Angewandte Chemie* **2017,** *129*, 7241.
24. Han, L.;Che, S. *Advanced Materials* **2018,** *30*, 1705708.
25. Ha, S.; La, Y.;Kim, K. T. *Accounts of Chemical Research* **2020,** *53*, 620.
26. La, Y.; Park, C.; Shin, T. J.; Joo, S. H.; Kang, S.;Kim, K. T. *Nature chemistry* **2014,** *6*, 534.
27. Glynos, E.; Pantazidis, C.;Sakellariou, G. *ACS omega* **2020,** *5*, 2531.
28. Galluzzo, M. D.; Loo, W. S.; Wang, A. A.; Walton, A.; Maslyn, J. A.;Balsara, N. P. *The Journal of Physical Chemistry B* **2020,** *124*, 921.

29. Hallinan Jr, D. T.;Balsara, N. P. *Annual review of materials research* **2013,** *43*, 503.
30. Li, Q.; Chen, C.; Li, C.; Liu, R.; Bi, S.; Zhang, P.; Zhou, Y.;Mai, Y. *ACS nano* **2020,** *14*, 13652.
31. Ito, Y.; Qiu, H. J.; Fujita, T.; Tanabe, Y.; Tanigaki, K.;Chen, M. *Advanced Materials* **2014,** *26*, 4145.
32. Lu, Z.; Li, C.; Han, J.; Zhang, F.; Liu, P.; Wang, H.; Wang, Z.; Cheng, C.; Chen, L.;Hirata, A. *Nature communications* **2018,** *9*, 276.
33. Matsen, M. W.;Bates, F. S. *The Journal of chemical physics* **1997,** *106*, 2436.
34. Liu, M.; Li, W.; Qiu, F.;Shi, A.-C. *Macromolecules* **2012,** *45*, 9522.
35. Meuler, A. J.; Hillmyer, M. A.;Bates, F. S. *Macromolecules* **2009,** *42*, 7221.
36. Bates, C. M.;Bates, F. S. *Macromolecules* **2017,** *50*, 3.
37. Wen, T.; Yuan, J.; Lai, W.; Liu, X.; Liu, Y.; Chen, L.;Jiang, X. *Macromolecules* **2022,** *55*, 4812.
38. Bates, F. S.;Fredrickson, G. H. *Annu. Rev. Phys. Chem.* **1990,** *41*, 525.
39. Bates, F. S.;Fredrickson, G. H. *Physics today* **1999,** *52*, 32.
40. Chen, J.; Thomas, E.; Ober, C.;Mao, G.-P. *Science* **1996,** *273*, 343.
41. Flynn, S. P.; Bogan, J.; Lundy, R.; Khalafalla, K. E.; Shaw, M.; Rodriguez, B. J.; Swift, P.; Daniels, S.; O'Connor, R.;Hughes, G. *Nanotechnology* **2018,** *29*, 355302.
42. Chung, T.-M.; Wang, H.-F.; Lin, T.; Chiang, Y.-W.; Chen, Y.-C.; Ko, B.-T.;Ho, R.-M. *Macromolecules* **2012,** *45*, 9727.
43. Cesteros, L. C.; Velada, J.;Katime, I. *Polymer* **1995,** *36*, 3183.
44. Eichhorn, K.-J.; Fahmi, A.; Adam, G.;Stamm, M. *Journal of molecular structure* **2003,** *661*, 161.
45. Jiang, Z.; Li, H.; He, Y.; Liu, Y.; Dong, C.;Zhu, P. *Applied Surface Science* **2019,** *479*, 765.
46. Müller, M.;Sun, D.-W. *Phys. Rev. Lett.* **2013,** *111*, 267801.
47. Condon, J. B., *Surface area and porosity determinations by physisorption: Measurement, classical theories and quantum theory*. Elsevier: 2006.
48. Kresge, C. T.; Leonowicz, M. E.; Roth, W. J.; Vartuli, J. C.;Beck, J. S. *Nature* **1992,** *359*, 710.
49. Li, Y.; Bastakoti, B. P.;Yamauchi, Y. *APL Materials* **2016,** *4*.
50. Zalusky, A. S.; Olayo-Valles, R.; Wolf, J. H.;Hillmyer, M. A. *Journal of the American Chemical Society* **2002,** *124*, 12761.
51. Sidorov, S. N.; Bronstein, L. M.; Kabachii, Y. A.; Valetsky, P. M.; Soo, P. L.; Maysinger, D.;Eisenberg, A. *Langmuir* **2004,** *20*, 3543.
52. Lin, T.; Li, C.-L.; Ho, R.-M.;Ho, J.-C. *Macromolecules* **2010,** *43*, 3383.
53. Fu, J.; Chen, Z.; Wang, M.; Liu, S.; Zhang, J.; Zhang, J.; Han, R.;Xu, Q. *Chemical Engineering Journal* **2015,** *259*, 53.